IEEE Access
Multidisciplinary ⋮ Rapid Review ⋮ Open Access Journal

Received 10 November 2022, accepted 11 December 2022, date of publication 15 December 2022,
date of current version 27 December 2022.

Digital Object Identifier 10.1109/ACCESS.2022.3229974

RESEARCH ARTICLE

Polarization Maintaining Fiber-Based Depth Encoded Cross-Polarized Optical Coherence Tomography

MARIA N. ROMODINA[1], KATHARINA BLESSING[1,2], AND KANWARPAL SINGH[1,2]
[1]Max Planck Institute for the Science of Light and Max-Planck-Zentrum für Physik und Medizin, 91058 Erlangen, Germany
[2]Department of Physics, Friedrich Alexander University Erlangen-Nürnberg, 91058 Erlangen, Germany

Corresponding author: Maria N. Romodina (maria.romodina@mpl.mpg.de)

This work was supported by the Max-Planck-Gesellschaft.

This work involved human subjects or animals in its research. Approval of all ethical and experimental procedures and protocols was granted by the Local Institutional Review Board of Ethikkommission der Friedrich-Alexander-Universität, Erlangen, Germany.

ABSTRACT Cross-polarized optical coherence tomography offers improved imaging contrast of birefringent tissue, such as collagen organization, compared to conventional optical coherence tomography systems. Therefore, it is a promising diagnostic tool for fibrosis and cancer. Existing cross-polarized optical coherence tomography systems require free-space polarization-controlling elements, which makes these systems bulky. In this work, we present a polarization-maintaining fiber-based minimalistic system for cross-polarization optical coherence tomography suitable for endoscopic applications. A long section of a polarization maintaining fiber is placed in the sample arm and acts as a delay line due to a large group-delay difference for two orthogonally polarized modes of the fiber. Co- and cross-polarized images appear at different depth positions within the image, providing a contrast enhancement due to visualization of the change of the light's polarization state in tissue. We demonstrate system designs for both benchtop and hand-held configurations. The images of a mouse's esophagus ex-vivo and the nailbed of a human volunteer are presented and reveal changes in the light's polarization state due to the presence of collagen in the tissue. The proposed all-fiber-based cross-polarized optical coherence tomography system has a high potential for endoscopy and can be translated to clinical applications.

INDEX TERMS Biomedical optical imaging, collagen, cross-polarized optical coherence tomography, endoscopic imaging, polarization-maintaining fiber.

I. INTRODUCTION

Optical coherence tomography (OCT) is an interferometric imaging technique, which has several diagnostic applications in the medical field [1], [2], in the studies of tissue and cell properties [3], and in microstructure metrology [4]. As an optical equivalent to ultrasound imaging, OCT opens the possibility to visualize tissue structures up to an imaging depth of a few mm and with a resolution of a few to tens of micrometers. OCT is widely used for early medical diagnosis. Some pathologies, however, provide better contrast with polarization-sensitive techniques [5], [6]. Fibrosis and stromal collagen organization, which are associated with the risk of a variety of cancers, can be detected by their birefringence and depolarization properties [7], [8]. Polarization-based OCT systems exploit the birefringence and depolarization properties of tissue to achieve additional contrast between different structures and, therefore, increase the possibility of an early-stage cancer diagnosis. Polarization-based OCT has been used to detect the ultrastructure of individual sarcomeres in muscle tissue [9], subretinal fibrosis [5], and to visualize and quantify airway smooth muscle during bronchoscopy [10], [11].

There are two types of polarization-based OCT techniques, polarization-sensitive OCT [12] (PS-OCT) and cross-polarized OCT [13] (CP-OCT). PS-OCT provides

The associate editor coordinating the review of this manuscript and approving it for publication was Szidonia Lefkovits.

a quantitative distribution of the birefringence and the optical axis orientation by analyzing the difference between images obtained from two orthogonally polarized light components [6], [14], [15].

CP-OCT, instead, provides two different contrast distributions, in the following named co- and cross-polarized images. Due to the sample's birefringence and scattering effects, the reflected light changes its polarization state [13]. The component of scattered light, which has the same polarization as the incident light, contributes to the co-polarized image. Another component with strictly orthogonal polarization contributes to the cross-polarized image. By the acquisition and comparison of the co- and cross-polarized images, it is possible to detect polarization change in birefringent tissue with structures such as collagen. The main advantage of the method is that the data acquisition does not require any prior knowledge of the optical axis orientation which simplifies its implementation compared to PS-OCT. However, it is impossible to separate the contributing polarization changing effects. Nevertheless, the different characteristics of co- and cross-polarized images found applications in different medical fields [16], [17], [18], [19].

Often, PS- and CP-OCT setups are built in free space which allows controlling the polarization states of the beams in reference and sample arms. However, for endoscopic applications, fiber-based approaches are required. In this case, the control of the polarization states becomes more complicated, because movements of single mode fibers (SMF) change the polarization state of the transmitted light in an unknown manner. Different input-polarization independent approaches were developed, based on building a free-space module with either a Faraday mirror [20] or a depolarizer and quarter-wave plates [21], [22], [23], [24]. However, these approaches contain free space elements, *i.e.* they are not all-fiber-based systems.

Polarization maintaining fibers (PMF) can be used to maintain linear polarization states in OCT systems. The PMF has two axes (a fast and a slow) that support the propagation of two orthogonal polarization modes through the fiber with high isolation. An interferometer only with PMFs was used to perform fiber-based PS-OCT [25], [26], [27]. PMFs were used instead of SMFs in both arms of the interferometer and two orthogonally polarized images were separated using a Wollaston prism in front of a spectrometer [26] or using a polarizing beam splitter and two detectors to record both images [27]. In other works, the PMF was used as a passive delay line to insert a time delay between the orthogonal modes and to separate the orthogonally polarized images [28], [29], [30]. Recently, S. Moon et al. proposed fiber-based PS-OCT in a minimalistic system configuration, in which a PMF is used in the sample arm right in front of the sample [31]. It was demonstrated that this technique is less sensitive to fiber probe motion compared to a standard SMF probe [32]. To perform polarization-sensitive measurements and to detect the optical axis orientation authors used a quarter wave plate between the fiber and the sample, which complicates the endoscopic realizations and increases the size of endoscopic probe [33]. This minimalistic system configuration can be adapted for CP-OCT instead of PS-OCT. An advantage is, that the system will work without QWP between the fiber and the sample and a simplified and compact endoscopic probe can be implemented.

In the present paper, we demonstrate a new method of PMF-based depth encoded CP-OCT. The PMF acts as a delay line and two orthogonally polarized images and one cross-polarized image appear at different depth positions within the OCT image. The proposed design is more suitable for endoscopic applications compared to the previously developed minimalistic PMF-based PS-OCT system [31] since no additional elements are used between the PMF and the sample. The cross-polarized image intensity is robust to probe fiber motion due to the high stability of the polarization state of light propagating through the PMF. We tested the system's performance in benchtop configuration, and show the sensitivity of the system to the birefringence properties of the sample by imaging a mouse esophagus. Further, we developed a hand-held endoscopic probe with the PMF and obtained in vivo images of the nail bed of a healthy volunteer. In both cases, the system provides enhanced contrast for birefringent tissue imaging.

II. MATERIALS AND METHODS

We did our research in two steps. First, we tested the concept on a benchtop system. Second, we created a hand-held probe to evaluate the perspective of endoscopic applications.

All the methods carried out in this work are in accordance with relevant guidelines and regulations from the local institutional review board (Ethikkommission der Friedrich-Alexander-Universität, Erlangen, Germany).

A. BENCHTOP SETUP

The schematic for the PMF-based CP-OCT setup is shown in Fig.1(A). We used a swept-source OCT system (Axsun Technologies, North Billerica, Massachusetts), with a laser sweeping range of 140 nm and a central wavelength of 1310 nm, and a sweep rate of 100 kHz. After applying a Hamming window to measured spectra a theoretical axial resolution of 6.2 μm is expected. The output power of the source is 24 mW. Additional to the illumination unit, the system comes with components for data acquisition, including a set of photodiodes to perform balance detection, and processing. The laser output is split using a 50/50 coupler and directed to the sample and the reference arm. Fiber polarization controllers are used to control the light's polarization in both the sample and the reference arm. In the reference arm, an additional SMF patch cable with a length of 5m is inserted to match the sample's optical path length. The light in the reference arm was collimated, reflected by the reference mirror, and coupled back into the

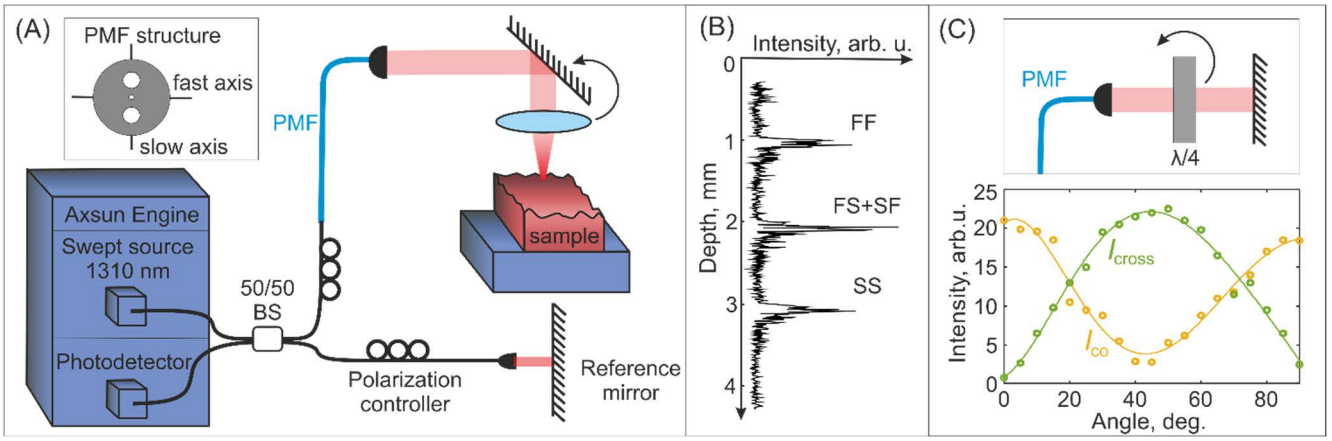

FIGURE 1. **(A) Schematic of the benchtop version of the experimental setup. (B) Typical A-scan for a paper, as a sample with a high depolarization ratio. Two co-polarized images are marked as FF and SS, cross-polarized image is marked as FS+SF. (C) The setup configuration for birefringence sensitivity test (top) and the light intensity for co- and cross-polarized images as a function of quarter-wave plate angle (bottom).**

fiber. In the sample arm, the light is coupled to a PMF (Thorlabs P3-1310PM-FC-5) with a length of 5 m. Measured power insertion losses due to the coupling from SMF to PMF and vice versa were lower than 7%. After the fiber, the light is collimated and focused on a sample using a lens with a NA=0.2. The theoretically expected lateral resolution is 4 μm, the experimentally measured value is 6 μm in the focal plane. The discrepancy can be explained by the slight divergence of the beam in the sample arm after the collimator. Experimentally measured axial resolution is 20 μm. The discrepancy between predicted and measured value appears due to dispersion mismatch between SMF in the reference arm and PMF in the sample arm. After algorithmic compensation of dispersion mismatch, an axial resolution of 10 μm was achieved. A galvanometer scanner accomplishes the lateral scanning of the sample. One B-scan acquisition time was 0.1 s.

In the sample arm, the PMF plays the role of a passive polarization delay unit. The PMF is highly birefringent with two eigenmodes with orthogonal linear polarizations. For one mode, the light is polarized along the fast axis and for another along the slow axis (see the inset of Fig. 1 (A)). The initial polarization state of the laser source is unknown, and some part of the light is coupled to the slow mode and some part is coupled to the fast mode. We measured the spectra of light coupled to slow and fast modes of the PMF and observed that the spectral shapes are similar for both modes and are not affected by the adjustment of polarization controllers. The birefringence of a sample alters the polarization state, the back-scattered light couples into the slow and fast. The speeds of light's propagation through the fiber are different for slow and fast modes. Thus, several images of the sample appear at different depths. Here, we denoted the 4 types of images:

- **SS** and **FF** are the co-polarized images, created by light, that propagates both ways in the slow or fast mode, correspondingly;
- **SF** and **FS** are the cross-polarized images. Instead of coupling back into the same mode after reflection, part of the signal couples into the opposite mode due to a change in polarization state after interaction with the sample.

Experimentally, we detected 3 depth-resolved images of the sample (see Fig.1 (B)). The light forming the **FF**-image has the lowest time delay concerning the light coming from the reference arm, therefore, the **FF**-image will appear closest to the zero optical delay line. The **SS**-image has the longest time delay and appears farthest in the A-scan. The depth separation can be calculated using the following equation:

$$\Delta D = \left(n_{slow} - n_{fast}\right) L,$$

where ΔD is the depth separation of **SS-** and **FF**- images, L is the length of the fiber, n_{slow} and n_{fast} are the refractive indexes for light propagation along the slow and fast axes. According to the vendor (Thorlabs Inc), the refractive index difference between the slow and the fast axis is approximately 0.00045. For 5m of PMF calculations provide $\Delta D = 2.25$mm. **SF**- and **FS**- images have the same time delay with respect to the light coming from the reference arm and appear as one combined cross-polarized image in the middle between the two co-polarized **SS-** and **FF**- images (see Fig. 1 (B)). Here, we defined the intensity pattern of the middle image (the sum of SF- and FS-images) as the cross-polarized image (I_{cross}). We calculate the co-polarized image signal (I_{co}) during the post-processing using the following equation:

$$I_{co} = \sqrt{I_{SS}^2 + I_{FF}^2},$$

where I_{SS} and I_{FF} are the intensity signals for **SS**- and **FS**-images, correspondingly. The total intensity signal (I) corresponding to the sample's reflectivity was calculated by the following equation:

$$I = \sqrt{I_{co}^2 + I_{cross}^2};$$

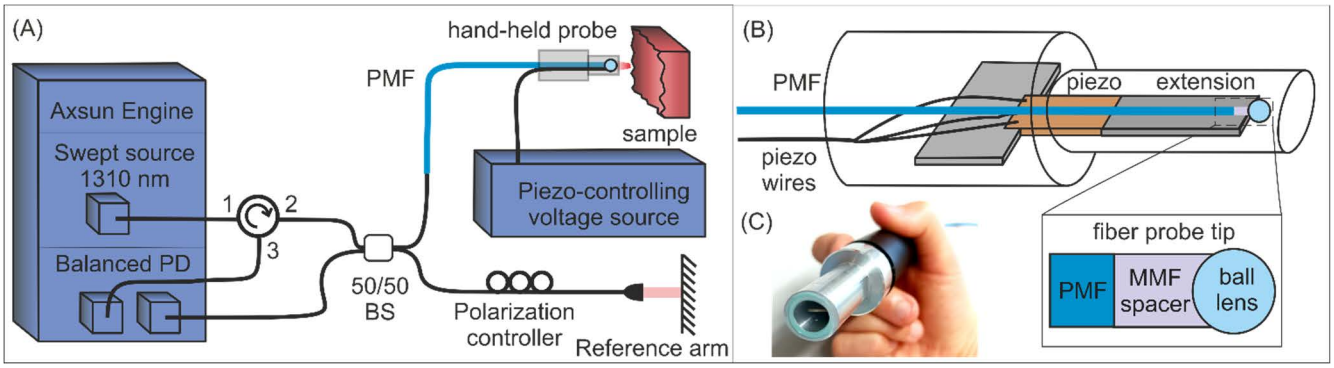

FIGURE 2. (A) The schematic of the hand-held version of experimental setup. (B) The schematic drawing of the hand-held probe and the fiber probe tip. (C) The photo of hand-held prob.

To highlight the differences between co- and cross-polarized images the contrast value $\delta = \frac{I_{cross}}{I_{cross}+I_{co}}$ has been calculated. Depolarization, retardance and diattenuation of light in a tissue contribute together to the changes of δ [13], [18], [22], which we name the cross-polarization ratio.

To test the system's sensitivity to the birefringent properties of the sample we used a mirror as a sample. In the experiment with mirror we observed a cross-talk of -30 dB between co-polarized and cross-polarized channels. We assume this cross-talk takes place because of a change of light's polarization due to the imperfection of galvo-mirrors and collimator surfaces. The cross-talk inside the PMF is ≤ -40 dB at 4 m, according to the data from the supplier, and can be neglected. We measured the sensitivity for different channels and obtained the following values of sensitivity: S_{FF}=89 dB, S_{SF+FS}=86 dB, and S_{SS}=83 dB for FF, SF+FS and SS images correspondingly. A 3-dB/mm sensitivity roll-off with the depth was observed. We used a polarization controller to compensate for SNR roll-off and make the signal for FF and SS channels equally bright.

In the test experiment we put a quarter waveplate (QWP) in the sample arm and measured the intensity of the mirror images as a function of the QWP's angle. The polarization of light in the reference and the sample arm was adjusted before the measurement to obtain the same brightness for **SS** and **FF** images. The graph in Figure 1(C) (bottom) shows the dependence of the light's intensity in co- (I_{co}) and cross-polarized (I_{cross}) images as a function of the QWP's angle. At an angle of 0°, the QWP is oriented along one of the axes of the PMF, and the light couples back to the PMF preserves the same polarization state. In this case, the co-polarized images of the mirror are maximally bright and the cross-polarized image is almost invisible. However, when the QWP is rotated 45°, the light coming from both axes changes its polarization to the opposite. In this case, the cross-polarized signal is maximal, while the signal for the co-polarized image is minimal. The results confirm that the system is sensitive to the birefringent properties of the sample, i.e. it pro vides the information about the change in the light's polarization due to the sample.

B. THE SETUP WITH THE HAND-HELD PROBE

To create an endoscopic version of the setup, we cut the ferrule from the PMF and attached an endoscopic probe to the end of the fiber. The endoscopic probe consists of a multimode fiber spacer of 500 μm for beam expansion and a ball lens with a diameter of 500 μm, which is glued to the end of the spacer. The beam waist of the focused beam was equal to 30 μm at a distance of 3 mm from the lens, corresponding to the lateral resolution. The endoscopic probe was fixed in a custom-designed tube with a piezo bender inside (Thorlabs PB4NB2S). A rigid plastic stripe with a length of 50 mm was glued to the piezo to extend the scanning range. The endoscopic probe was fixed on the plastic stripe. Lateral scanning within the range of 3 mm was performed by applying an alternating voltage to the piezo bender. Additionally, a circulator was added before the beam splitter and balanced detection was used to improve the image quality and reduce the noise. We measured the sensitivity for different channels in the hand-held probe and obtained the following results: S_{FF}=86 dB, S_{SF+FS}=83 dB, and S_{SS}=80 dB. The endoscopic probe has a 3 dB lower sensitivity compared to the benchtop setup due to the lower collection efficiency of the ball lens.

III. RESULTS

In figure 3, we show a single frame of an ex-vivo image of a mouse esophagus obtained using the benchtop PMF-based CP-OCT system. In the co-polarized image, the top epithelial layer is brighter than the lower part of the tissue. It happens because the epithelial layer has a low retardance and barely changes the polarization state of the light [30]. The maximum polarization change is observed for the lamina propria layer due to the presence of collagen, thus in the cross-polarized image, the deeper layer shows more signal. From the image of the depolarization ratio distribution, the border between the epithelium and the lamina propria can be detected.

In Figure 4, we show a single-frame image of a nailbed from a healthy volunteer, obtained using a hand-held probe. No approval from the Ethics committee is required for

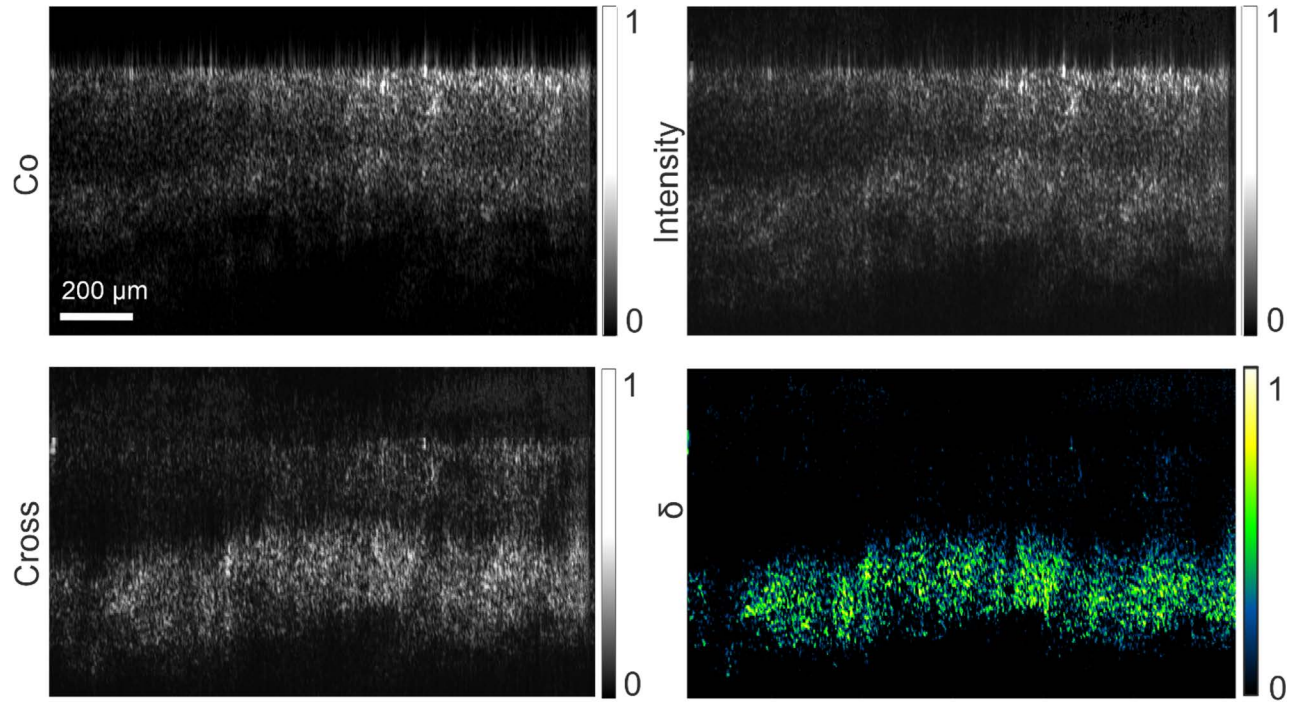

FIGURE 3. OCT images of ex-vivo mouse esophagus tissue acquired with benchtop PMF-based CP-OCT system. Co-polarized image, cross-polarized image, total intensity image and the depolarization ratio distribution are shown in the figure. The values of intensity, co- and cross-signals in the images were normalized to the maximal value, scale bar corresponds for both axes.

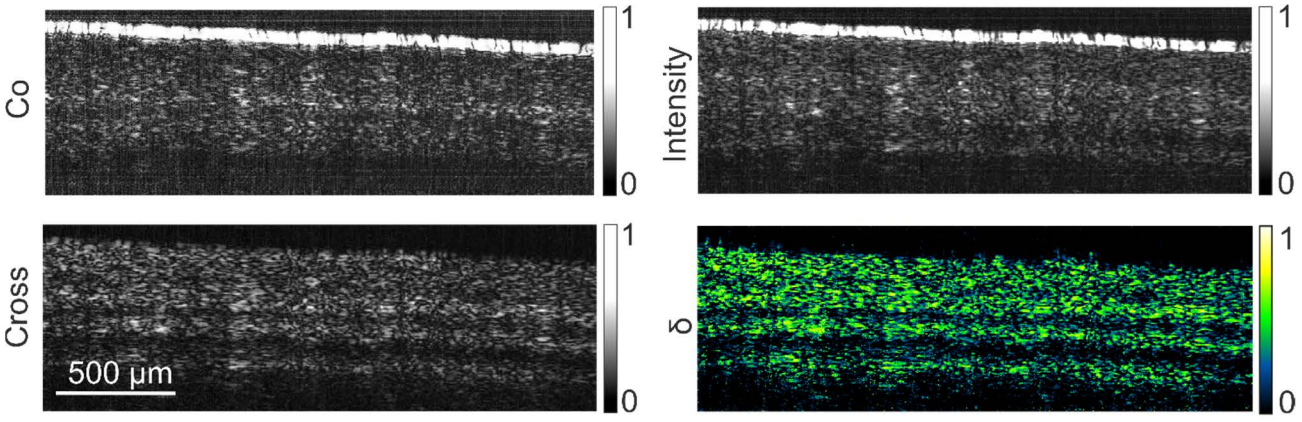

FIGURE 4. In-vivo nail bed images acquired with a hand-held PMF-based CP-OCT probe. Co-polarized image, cross-polarized image, total intensity image and the depolarization ratio distribution are shown in this figure. The values of of intensity, co- and cross-signals in the images were normalized to the maximal value, scale bar corresponds for both axes.

such an imaging procedure. The co-polarized image shows a very strong reflection from the top surface, while the cross-polarized image has a signal only from the deeper region of the nail. Both co- and cross-polarized images demonstrate a characteristic striped pattern. The strong birefringence properties of the collagen paired with its degree of organization in the nail lead to the appearing of the striped pattern. The polarization of the light changes over its propagation through a birefringent material. Thus, it changes periodically with the depth of the sample. For one depth position, the co-polarized signal has a minimum while the cross-polarized signal has a maximum. For another depth position, the situation is the opposite. This behavior is more evident in the lower right image where we show the pixelwise distribution of the depolarization ratio because it provides higher contrast for polarization changes in collagen imaging.

IV. DISCUSSION

A simple all-fiber CP-OCT technique is demonstrated for both benchtop and hand-held probe implementations. Compared to previous CP-OCT systems, it has a depth-encoded all-fiber design without free-space elements for

polarization control. Due to the high mode stability in PMFs the imaging is not sensitive to the fiber probe motion [32]. In comparison to many previously reported endoscopic cross-polarized systems, our current approach provides both co- and cross-signal in one shot. We demonstrate a hand-held realization of the technique and show that the system is suitable for endoscopic applications since no additional optical elements are used between the PMF and the sample. We observed a slightly lower sensitivity for the endoscopic probe compared to the benchtop system. This takes place due to the lower collection efficiency of the probe compared to the benchtop system.

Despite the listed advantages, the system has some limitations. First of all, the provided technique is not polarization insensitive, and the brightness of the images can be distorted by the motion of the system's single-mode fibers. This can be prevented by fixing all fibers except the PMF in the hand-held probe. To see a high contrast for depolarization and a strong signal in the cross-polarized image, one should control the polarization state of the light in the sample and reference arm. The best imaging quality is obtained, when approximately half of the light is polarized along the slow axis and the second half is polarized along the fast axis of the PMF. However, the adjustment of the polarization is not complicated and can be done using a fiber polarization controller during the imaging procedure. Another limitation of the system is, that the depth separation between the images cannot be adjusted during measurements and is defined by the length of the PMF. Also, there is a reduction of the imaging depth range due to the depth-multiplexing scheme. This however can be compensated using systems with longer imaging depth and longer section of PMF.

V. CONCLUSION

For the first time, we proposed a simple all-fiber-based CP-OCT system with a long PMF to detect depth-encoded polarization-multiplexed signals. The concept of the system was tested using a benchtop configuration. Test measurements with a quarter-wave plate demonstrate the sensitivity of the system to the birefringence of the sample. The images for mouse esophagus ex-vivo tissue demonstrate the ability of the system to provide enhanced contrast and resolve the top epithelium layer and the layer of the lamina propria. The PMF-based hand-held probe was developed to demonstrate the feasibility of the proposed technique for endoscopic applications. Using the hand-held probe, we imaged the nailbed of a human volunteer. Obtained images show the characteristic laminar structure, which corresponds to the birefringent properties of the collagen in the nail.We believe that in the future PMF-based CP-OCT endoscopic probes can be useful for high contrast in-vivo imaging of collagen organization, which is associated with cancer progression.

REFERENCES

[1] D. Huang, "Optical coherence tomography," *Science*, vol. 254, no. 5035, pp. 1178–1181, 1991.
[2] H. Zhang, C. Wu, M. Singh, A. Nair, S. R. Aglyamov, and K. V. Larin, "Optical coherence elastography of cold cataract in porcine lens," *J. Biomed. Opt.*, vol. 24, no. 3, Mar. 2019, Art. no. 036004.
[3] M. A. Sirotin, M. N. Romodina, E. V. Lyubin, I. V. Soboleva, and A. A. Fedyanin, "Single-cell all-optical coherence elastography with optical tweezers," *Biomed. Opt. Exp.*, vol. 13, no. 1, pp. 14–25, 2022.
[4] K. R. Safronov, V. O. Bessonov, D. V. Akhremenkov, M. A. Sirotin, M. N. Romodina, E. V. Lyubin, I. V. Soboleva, and A. A. Fedyanin, "Miniature Otto prism coupler for integrated photonics," *Laser Photon. Rev.*, vol. 16, no. 4, Apr. 2022, Art. no. 2100542.
[5] M. G. O. Gräfe, J. A. van de Kreeke, J. Willemse, B. Braaf, Y. de Jong, H. S. Tan, F. D. Verbraak, and J. F. de Boer, "Subretinal fibrosis detection using polarization sensitive optical coherence tomography," *Transl. Vis. Sci. Technol.*, vol. 9, no. 4, p. 13, Mar. 2020.
[6] J. F. D. Boer, C. K. Hitzenberger, and Y. Yasuno, "Polarization sensitive optical coherence tomography-a review," *Biomed. Opt. Exp.*, vol. 8, no. 3, pp. 1838–1873, 2017.
[7] A. Devendra, K. C. Niranjan, A. Swetha, and H. Kaveri, "Histochemical analysis of collagen reorganization at the invasive front of oral squamous cell carcinoma tumors," *J. Investigative Clin. Dentistry*, vol. 9, no. 1, Feb. 2018, Art. no. e12283.
[8] J. Walther, "Depth-resolved birefringence imaging of collagen fiber organization in the human oral mucosa in vivo," *Biomed. Opt. Exp.*, vol. 10, no. 4, pp. 1942–1956, 2019.
[9] J. J. Pasquesi, S. C. Schlachter, M. D. Boppart, E. Chaney, S. J. Kaufman, and S. A. Boppart, "In vivo detection of exercise-induced ultrastructural changes in genetically-altered murine skeletal muscle using polarization-sensitive optical coherence tomography," *Opt. Exp.*, vol. 14, no. 4, pp. 1547–1556, 2006.
[10] M. Vaselli, P. C. Wijsman, J. Willemse, A. W. M. Goorsenberg, F. Feroldi, J. N. S. d'Hooghe, J. T. Annema, J. F. de Boer, and P. I. Bonta, "Polarization sensitive optical coherence tomography for bronchoscopic airway smooth muscle detection in bronchial thermoplasty-treated patients with asthma," *Chest*, vol. 160, no. 2, pp. 432–435, Aug. 2021.
[11] J. Willemse, "Polarization-sensitive optical coherence tomography in end-stage lung diseases: An ex vivo pilot study," *Biomed. Opt. Exp.*, vol. 12, no. 11, pp. 6796–6813, 2021.
[12] M. R. Hee, D. Huang, E. A. Swanson, and J. G. Fujimoto, "Polarization-sensitive low-coherence reflectometer for birefringence characterization and ranging," *J. Opt. Soc. Amer. B, Opt. Phys.*, vol. 9, no. 6, pp. 903–908, 1992.
[13] J. M. Schmitt and S. H. Xiang, "Cross-polarized backscatter in optical coherence tomography of biological tissue," *Opt. Lett.*, vol. 23, no. 13, pp. 1060–1062, 1998.
[14] J. F. de Boer and T. E. Milner, "Review of polarization sensitive optical coherence tomography and Stokes vector determination," *J. Biomed. Opt.*, vol. 7, no. 3, pp. 359–371, 2002.
[15] B. Baumann, "Polarization sensitive optical coherence tomography: A review of technology and applications," *Appl. Sci.*, vol. 7, no. 5, p. 474, May 2017.
[16] K. S. Yashin, E. B. Kiseleva, E. V. Gubarkova, A. A. Moiseev, S. S. Kuznetsov, P. A. Shilyagin, G. V. Gelikonov, I. A. Medyanik, L. Y. Kravets, A. A. Potapov, E. V. Zagaynova, and N. D. Gladkova, "Cross-polarization optical coherence tomography for brain tumor imaging," *Frontiers Oncol.*, vol. 9, pp. 1–13, Apr. 2019.
[17] X. Yao, Y. Gan, Y. Ling, C. C. Marboe, and C. P. Hendon, "Multicontrast endomyocardial imaging by single-channel high-resolution cross-polarization optical coherence tomography," *J. Biophoton.*, vol. 11, no. 4, Apr. 2018, Art. no. e201700204.
[18] E. V. Gubarkova, M. Y. Kirillin, V. V. Dudenkova, P. S. Timashev, S. L. Kotova, E. B. Kiseleva, L. B. Timofeeva, G. V. Belkova, A. B. Solovieva, A. A. Moiseev, G. V. Gelikonov, I. I. Fiks, F. I. Feldchtein, and N. D. Gladkova, "Quantitative evaluation of atherosclerotic plaques using cross-polarization optical coherence tomography, nonlinear, and atomic force microscopy," *J. Biomed. Opt.*, vol. 21, no. 12, Dec. 2016, Art. no. 126010.
[19] P. Lenton, J. Rudney, A. Fok, and R. S. Jones, "Clinical cross-polarization optical coherence tomography assessment of subsurface enamel below dental resin composite restorations," *J. Med. Imag.*, vol. 1, no. 1, May 2014, Art. no. 016001.
[20] K. Blessing, J. Schirmer, A. Parmar, and K. Singh, "Depth encoded input polarisation independent swept source cross-polarised optical coherence tomography probe," *J. Phys. D, Appl. Phys.*, vol. 54, no. 30, 2021, Art. no. 305401.

[21] K. Blessing, J. Schirmer, G. Sharma, and K. Singh, "Novel input polarisation independent endoscopic cross-polarised optical coherence tomography probe," *J. Biophoton.*, vol. 13, no. 12, Dec. 2020, Art. no. 202000134.
[22] G. Sharma, S. Sharma, K. Blessing, G. Hartl, M. Waldner, and K. Singh, "Swept source cross-polarized optical coherence tomography for any input polarized light," *J. Opt.*, vol. 22, no. 4, Apr. 2020, Art. no. 045301.
[23] G. R. Hartl, A. Parmar, G. Sharma, and K. Singh, "Cross-polarized optical coherence tomography system with unpolarized light," *Photonics*, vol. 9, no. 2, p. 76, Jan. 2022.
[24] S. Sharma, G. Hartl, S. K. Naveed, K. Blessing, G. Sharma, and K. Singh, "Input polarization-independent polarization-sensitive optical coherence tomography using a depolarizer," *Rev. Sci. Instrum.*, vol. 91, no. 4, Apr. 2020, Art. no. 043706.
[25] M. K. Al-Qaisi and T. Akkin, "Swept-source polarization-sensitive optical coherence tomography based on polarization-maintaining fiber," *Opt. Exp.*, vol. 18, no. 4, pp. 3392–3403, 2010.
[26] H. Wang, M. K. Al-Qaisi, and T. Akkin, "Polarization-maintaining fiber based polarization-sensitive optical coherence tomography in spectral domain," *Opt. Lett.*, vol. 35, no. 2, p. 154, 2010.
[27] E. Götzinger, B. Bernhard, P. Michael, and C. K. Hitzenberger, "Polarization maintaining fiber based ultra-high resolution spectral domain polarization sensitive optical coherence tomography," *Opt. Exp.*, vol. 17, no. 25, pp. 22704–22717, 2009.
[28] B. Baumann, W. Choi, B. Potsaid, D. Huang, J. S. Duker, and J. G. Fujimoto, "Swept source/Fourier domain polarization sensitive optical coherence tomography with a passive polarization delay unit," *Opt. Exp.*, vol. 20, no. 9, pp. 10218–10230, 2012.
[29] L. Cahill, A. M. Lee, H. Pahlevaninezhad, S. Ng, C. E. MacAulay, C. Poh, and P. Lane, "Passive endoscopic polarization sensitive optical coherence tomography with completely fiber based optical components," *Proc. SPIE*, vol. 9304, pp. 55–62, Mar. 2015.
[30] Z. Wang, "Depth-encoded all-fiber swept source polarization sensitive OCT," *Biomed. Opt. Exp.*, vol. 5, no. 9, pp. 2931–2949, 2014.
[31] S. Moon, Y. Miao, and S. Chen, "Fiber-based polarization-sensitive optical coherence tomography of a minimalistic system configuration," *Opt. Lett.*, vol. 44, no. 12, pp. 3150–3153, 2019.
[32] Z. Lu and C. Liu, "Fiber motion-insensitive fiber-based polarization-sensitive optical coherence tomography for optic axis determination," *JOSA B*, vol. 37, no. 3, pp. 608–617, 2020.
[33] Y. Li, S. Moon, Y. Jiang, S. Qiu, and Z. Chen, "Intravascular polarization-sensitive optical coherence tomography based on polarization mode delay," *Sci. Rep.*, vol. 12, no. 1, pp. 1–9, Apr. 2022.

MARIA N. ROMODINA received the Ph.D. degree from Lomonosov Moscow State University, Russia, in 2018. She is a Postdoctoral Fellow with the Max Planck Institute for the Physics of Light, Germany. Her current research interests include the development of novel miniaturized devices for optical coherence tomography and Brillouin imaging.

KATHARINA BLESSING received the Diploma degree in physics from the University of Ulm, Germany. She is currently pursuing the Ph.D. degree with the Max Planck Institute for the Science of Light, Erlangen, Germany. Her current research interest includes clinical applications of cross-polarized optical endo-tomography.

KANWARPAL SINGH received the Ph.D. degree from INRS, Canada, in 2013. He was a Postdoctoral Fellow at Harvard Medical School, USA, until 2018, where he worked on the development of high-resolution optical coherence tomography systems. He is a Leader with the Independent Research Group (Microendoscopy), Max Planck Institute for the Science of Light, Germany. His research interest includes the development of miniaturized flexible endoscopic devices for imaging inside the body.